metals

MDPI

Article

Phase Formation and Stabilization Behavior of Ca-PSZ by Post-Heat Treatment II: CaOx-ZrO_2(1 − x) (x = 5–10 mol%)

Hyunjo Yoo [1,†], Juyoung Kim [1,†], Hwanseok Lee [2], Ilguk Jo [3,*] and Heesoo Lee [2,*]

[1] School of Convergence Science, Pusan National University, Busan 46241, Republic of Korea; hyunjoyoo@pusan.ac.kr (H.Y.); juyoungkim@pusan.ac.kr (J.K.)
[2] School of Materials Science and Engineering, Pusan National University, Busan 46241, Republic of Korea; hwanseok@pusan.ac.kr
[3] Department of Advanced Materials Engineering, Dong-Eui University, Busan 47340, Republic of Korea
* Correspondence: ijo@deu.ac.kr (I.J.); heesoo@pusan.ac.kr (H.L.); Tel.: +82-51-890-1698 (I.J.); +82-51-510-2388 (H.L.)
† These authors contributed equally to this work.

Abstract: The effects of CaO content and post-heat treatment were investigated on the phase stability and mechanical and thermal properties of Ca-PSZ. ZrO_2 specimens with 5–10 mol% CaO were sintered, and post-heat treatment was performed at 1200 °C for 100 h. Subsequently, to test and analyze the crystal structure and the microstructure, the mechanical and thermal properties of the specimens were evaluated. All specimens were partially stabilized by 5–10 mol% CaO (5CSZ–10CSZ) in a mixed monoclinic and tetragonal phase; however, peaks of the secondary phase of $CaZrO_3$ were observed in 10CSZ. The ratio of the monoclinic phase decreased from 62.50% (5CSZ) to 21.02% (10CSZ) as the CaO content increased. Additionally, the monoclinic phase ratio decreased from 59.38% (5CSZ) to 19.57% (9CSZ) after the post-heat treatment; an increase to 24.84% was observed for 10CSZ. An increase in Vickers hardness from 676.02 to 1256.25 HV and flexural strength from 437.7 to 842.7 MPa was observed with increasing CaO content. The post-heat treatment resulted in further increases in these values as the CaO content increased from 5CSZ to 9CSZ; however, the Vickers hardness and flexural strength of 10CSZ decreased by approximately 8% and 9%, respectively. The thermal expansion coefficient exhibited the same tendency as the mechanical properties. This coefficient increased from 8.229 × 10^{-6} to 9.448 × 10^{-6} K^{-1} with increasing CaO content and was enhanced after the post-heat treatment in 5CSZ to 9CSZ; however, the thermal expansion coefficient of 10CSZ decreased by approximately 4% after the post-heat treatment. The mechanically and thermally stable tetragonal phase increased, and the monoclinic phase decreased as the doped Ca replaced the Zr sites, as was confirmed by the X-ray diffraction (XRD) analysis. The post-heat treatment and the increased Ca addition further facilitated the replacement of Zr sites by Ca. However, at high Ca concentrations of 10CSZ, an equilibrium phase of $CaZrO_3$ was formed as a secondary phase at the post-heat treatment temperature, resulting in low performance.

Keywords: calcined partially stabilized zirconia; porous material; submerged entry nozzle; CaO content; post-heat treatment; phase transition; phase volume fraction; thermal expansion; mechanical properties

check for updates

Citation: Yoo, H.; Kim, J.; Lee, H.; Jo, I.; Lee, H. Phase Formation and Stabilization Behavior of Ca-PSZ by Post-Heat Treatment II: CaOx-ZrO_2(1 − x) (x = 5–10 mol%). *Metals* **2023**, *13*, 1659. https://doi.org/10.3390/met13101659

Academic Editor: Jiri Svoboda

Received: 11 September 2023
Revised: 22 September 2023
Accepted: 25 September 2023
Published: 27 September 2023

Copyright: © 2023 by the authors. Licensee MDPI, Basel, Switzerland. This article is an open access article distributed under the terms and conditions of the Creative Commons Attribution (CC BY) license (https://creativecommons.org/licenses/by/4.0/).

1. Introduction

The fourth industrial revolution is characterized by the convergence of advanced high technologies, for example, smart technology, artificial intelligence, advanced robotics, and the Internet of Things, with industrial processes. These state-of-the-art technologies cannot be implemented without the support of hardware elements, and there is a need to develop high-tech materials that meet more diverse and improved performance requirements than ever [1,2]. Ultra-light, ultra-hard, and ultra-high heat-resistant materials are required in movement- and transport-related fields such as aerospace and automotive industries.

In addition, in the fields of electronics and biotechnology, complex microscale materials with electrical and insulating properties are sometimes required. Since these are the characteristics that cannot be satisfied with conventional materials, such as metals, ceramics, and polymers that can be obtained from nature, the development of advanced materials with much more diverse and improved performance is required to achieve industrial advancement in the future. Thus, unlike conventional materials found in nature, advanced materials are precisely adjusted materials based on a refined or synthesized raw material, and numerous studies have been conducted in various research and development fields recently for the development of new advanced materials [3–5].

One of the required properties of the advanced materials is the capacity to withstand extreme conditions, such as high temperatures and corrosive environments. Zirconia (ZrO_2) has been widely studied because of its excellent mechanical, thermal, and chemical properties even in extremely harsh environment. Especially because despite being a ceramic, it has high toughness comparable to that of a metal; thus, it can be used as a suitable alternative in various fields of material development, such as for structural and functional applications [6–9]. Depending on the temperature, the crystal structure and mechanical properties of zirconia can be significantly altered. When it is used at high temperatures for long periods, the tetragonal phase of zirconia transforms into a monoclinic phase. That phenomenon is called the martensitic transformation effect (transformation of the tetragonal phase to the monoclinic phase), and it occurs in high-temperature applications resulting in volume expansion and toughness degradation. Consequently, cracks and intergranular fractures are formed because of the expanding volume, resulting in a rapid reduction in strength [10–12].

Various studies have been conducted to improve the mechanical and thermal properties of zirconia for high-temperature applications by using compounds, such as Y_2O_3, MgO, Al_2O_3, Bi_2O_3, and CaO, as stabilizers of the zirconia phase [13,14]. Doping of these stabilizers induces stabilization by reducing the c/a lattice constant ratio of zirconia on the tetragonal to form a structure with low residual stress inside the lattice by reducing distortion in the tetragonal phase [15,16]. Based on the type and concentration of the stabilizer, zirconia can be partially (partially stabilized zirconia, PSZ) to fully stabilized (fully stabilized zirconia, FSZ) at high temperatures. Since the PSZ and FSZ absorb the stress generated when a crack occurs and change into a monoclinic phase, they can obtain an increase in mechanical strength. Thus, the degree of zirconia stabilization is affected by the type, quantity, and heat treatment of the stabilizer [17–19]. Yttria-stabilized zirconia (YSZ) is the most famous in the fields of electricity and biotechnology. Depending on the doping amount of yttria stabilizer, the electrical and mechanical properties of YSZ have been significantly altered. According to existing research, 3 mol% YSZ can be used for electrolyte, and 8 mol% YSZ can be used for dental applications [9,19–21]. Magnesia-stabilized zirconia (MgPSZ) can act as partially stabilized zirconia due to the solubility of Mg to Zr and is famous for its use in structural ceramics, such as refractories [22].

Compared with other types stabilized zirconia, CaO-doped zirconia (CaO partially stabilized zirconia, Ca-PSZ) exhibits excellent mechanical properties in high temperature conditions, such as high hardness and high-temperature oxidation resistance; thus, it is used in a wide range of applications such as electrical insulators, fuel cells, and bioceramics. It is incorporated in refractory materials that require high mechanical properties at high temperature [23–27]. Although Ca-PSZ exhibits enhanced mechanical and thermal properties, repeated long-term use at ultra-high temperatures (>1500 °C) destabilizes Ca. Therefore, there is a need for research that can prevent the destabilization of Ca-PSZ and enhance its mechanical and thermal properties. Such research should be conducted first to investigate the mechanical thermal properties of Ca-PSZ according to the Ca content, then to study the ways to prevent the destabilization of Ca and improve the performance parameters.

A previous study showed that the mechanical properties of Ca-PSZ improved as the Ca content increased from 1 to 5 mol% [28]. The TEM analysis was performed and showed that the enhanced mechanical and thermal properties might be affected by a decrease in the

volume fraction of the monoclinic phase, even though the volume fraction of 5CSZ was over 50%. Thus, there are still possibilities to improve the mechanical and thermal properties of Ca-PSZ, and the effect of the Ca content higher than 5 mol% must be investigated. In this study, Ca-PSZ was synthesized using a conventional solid-state synthesis method by adding 5–10 mol% CaO with the subsequent post-heat treatment of the sintered samples and to further improve its properties. The crystal structure and microstructure of Ca-PSZ were analyzed based on its CaO content and the post-heat treatment. The Vickers hardness and flexural strength were measured to evaluate the mechanical properties of Ca-PSZ. The thermal expansion coefficient was measured as a thermal property.

2. Experimental Procedure

The Ca-PSZ specimens were fabricated by a solid-state synthesis method using two starting materials, ZrO_2 (99%, Daejung Chemicals & Metals Cooperation) and CaO (98%, Junsei Chemical Cooperation) powders. The composition of CaO varied by 5~10 mol%. Starting materials were prepared by stoichiometric calculation and were mixed by wet ball-milling method for 24 h using zirconia balls and ethanol. Mixed solutions were then dried at 100 °C for 24 h using a dry oven and were calcined at 1200 °C for 2 h in a box-type electric furnace.

The green body was prepared with calcined powders by uniaxially exerting a pressure of 1 Mg/cm^3 on the Ca-PSZ powder to form cylindrical (20 mm diameter) and rod-like (5 mm width, 35 mm height) shapes. Subsequently, the samples were sintered at 1600 °C for 6 h using an electric furnace and then cooled by air to room temperature. Sintered specimens were heated again at 1200 °C for 100 h as post-heat treatment using an electric furnace.

All the measurements were evaluated using the following measurements before and after the post-heat treatment. Phase transformation was observed using a powder X-ray diffraction method (XRD, Rigaku, Ultima-IV, Akishima, Japan). This method used Cu Kα as the X-ray source and implemented a scanning range of 20° to 80° at 0.02°/2θ step and a scanning speed of 2°/min. The peaks of materials and phase volume fraction were analyzed by Equation (1) and the Rietveld refinement method using Highscore plus software. Microstructural analysis was performed using field emission scanning electron microscopy (FE-SEM, MIRA3, TESCAN, Brno, Czech Republic) at the Converging Materials Core Facility. Thermomechanical analysis (TMA450, Ta Instruments, New Castle, United States) was used to measure the temperature range from 30 to 1000 °C at 5.0 °C/min; this was used to assess the behavior of the thermal expansion coefficient. Mechanical properties were evaluated using Vickers hardness and flexural strength tests. Vickers hardness was determined using a micro Vickers hardness tester (Wilson@VH1102, Buehler, IL, United States). Measurements were performed under 20 N for 15 s. The average value of 10 measurements was used to calculate the Vickers hardness. To measure the flexural strength of each specimen, a universal testing machine (United States) was used to measure the three-point flexural strength at a lower support-point distance of 20 mm and crosshead speed of 0.5 mm/min.

3. Results and Discussions

Figure 1 displays the results of the XRD analysis of the Ca-PSZ specimens, which contained varying quantities of CaO (5, 6, 7, 8, 9, and 10 mol%). A tetragonal and monoclinic mixed phase was observed in all specimens shown in Figure 1a,b. However, $CaZrO_3$, the second phase of Ca-PSZ, appeared only in the case of 10 CSZ after the post-heat treatment (see Figure 1b for 10 CSZ). The volume fraction of Ca-PSZ was quantified by calculating the peak intensity with Equation (1) derived by Potter and Heuer [29].

$$V_m = \frac{I\left(111\right)_m + I(111)_m}{I\left(111\right)_m + I(111)_m + I(101)_t} \quad (1)$$

where V_m represents the volume fraction of the monoclinic phase, and I represents the intensity of the XRD peaks of the monoclinic and tetragonal phases.

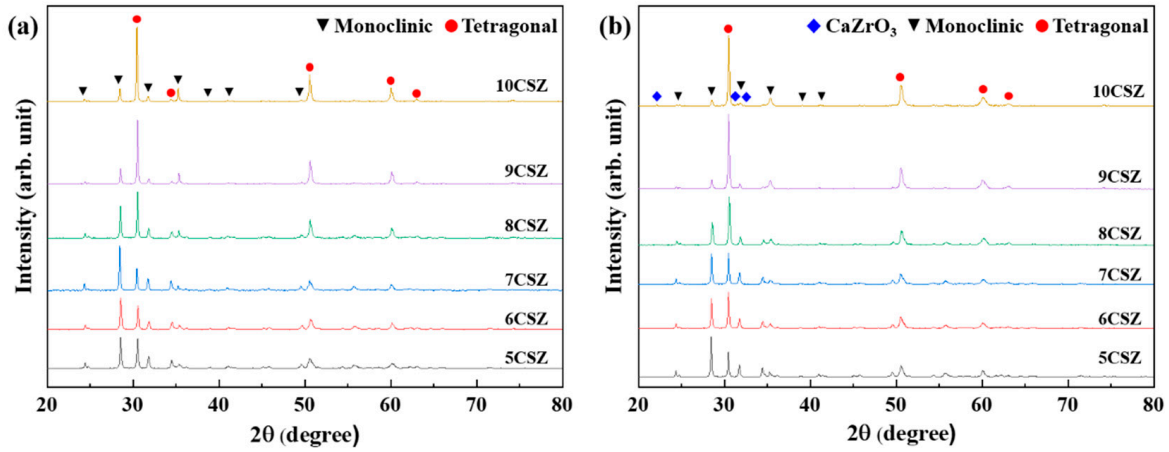


Figure 1. XRD patterns of Ca-PSZ specimens, which contained varying quantities of CaO (5, 6, 7, 8, 9, and 10 mol%), (**a**) before and (**b**) after post-heat treatment.

An increase in the CaO content before and after the post-heat treatment was associated with a reduction in the monoclinic peak at 31.8° and an increase in the tetragonal peak at 30.5°. This was corroborated by V_m of Ca-PSZ in Table 1. The V_m value of 5CSZ was 62.5% before the post-heat treatment and 59.38% after the post-heat treatment. These results are consistent with the findings of the previous study [28]. An increase in the amount of added CaO reduced V_m from 5CSZ (62.50%) to 10CSZ (21.02%) before the post-heat treatment. The post-heat treatment further reduced V_m from 5CSZ (62.50% to 59.38%) to 9CSZ (31.55% to 19.57%), and the V_m value of 9CSZ exhibited the largest reduction (approximately 38%). All the results of V_m measurements were lower than those for 2CSZ to 5CSZ [28], as expected. These findings indicate that increasing the quantity of CaO enhances the substitution of Zr^{4+} sites by Ca^{2+}. This affected the stabilization of Ca-PSZ by transforming the monoclinic phase into the tetragonal phase. Furthermore, the post-heat treatment accelerated the diffusion of Ca into the zirconia grains without precipitation at the grain boundary, resulting in a reduction in the monoclinic phase [28]. However, the V_m value of 10CSZ increased from 21.02% to 24.84% after the post-heat treatment, and the $CaZrO_3$ phase was observed. It is believed that the formation of the $CaZrO_3$ phase, a balanced phase at high temperature over 1200 °C and containing higher CaO content than the target phase of $Ca_xZr_{(1-x)}O_3$ (x = 0.1), occurred due to the imbalance of the CaO content in the Ca-PSZ system at the temperature of the post-heat treatment. As a result, the ratio of the monoclinic phase increased and caused the destabilization of Ca-PSZ by reducing the stable tetragonal phase in the case of 10CSZ, which had the CaO content higher than 10 mol% [30].

Table 1. Volume fraction of Ca-PSZ monoclinic phase.

Specimen	Volume Fraction of the Monoclinic Phase (%, V_m)	
	Before Post-Heat Treatment	After Post-Heat Treatment
5CSZ	62.50	59.38
6CSZ	58.23	55.02
7CSZ	52.22	47.25
8CSZ	43.54	37.21
9CSZ	31.55	19.57
10CSZ	21.02	24.84

The surface morphology of the Ca-PSZ specimens are shown in Figures 2 and 3. Grain size was measured by analyzing the SEM images based on ISO 13383-1. An increase in the CaO content and post-heat treatment had no visible effect on the grain size of specimens, and most of grain sizes were about 2.39 μm, similar to those in 5CSZ to 7CSZ (see (a) to (c) of Figures 2 and 3). In contrast, the 8CSZ showed a larger grain size of 2.63 μm, about 10% larger than that of 5CSZ to 7CSZ; furthermore, 9CSZ and 10CSZ showed a much larger grain size of 3.64 and 4.41 μm, respectively. The high Ca content also resulted in a large deviation from the grain size distribution as shown in Figure 2e,f. Additionally, the grain sizes of the 9CSZ and 10 CSZ increased to approximately 4.6% (3.81 μm) and 3.2% (4.55 μm) after the post-heat treatment, which was different from the specimens 5CSZ to 8CSZ that had no significant changes. As the added amount of Ca increases, the oxygen capacity also increases because Ca^{2+} replaces more of Zr^{4+}, which is known to be related to the increase in the grain size [31]. However, if more than 10 mol% of Ca is added, the excess amount of the added Ca could not be dissolved and precipitated into the small grains shown in Figures 2f and 3f. The post-heat treatment for this condition is expected to initiate the precipitation of the secondary phase of $CaZrO_3$, accelerate the precipitation, and destabilize the Ca-PSZ. As a result, it is believed that an increase in the Ca content and post-heat treatment affected the grain size growth in specimens with high CaO contents. In addition, the post-heat treatment at 1200 °C, which is a tetragonal–monoclinic transformation temperature, activated two different driving forces: densification from 5CSZ to 8CSZ with small average particle size differences and coarsening, which is more dominant in 9CSZ and 10CSZ with relatively large particles.

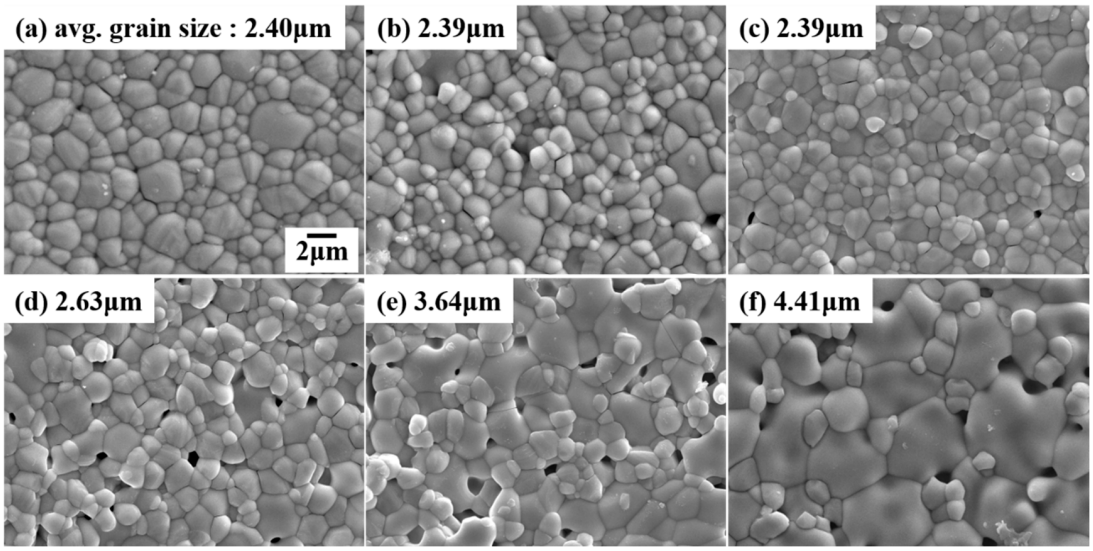


Figure 2. FE-SEM images and average grain sizes of (**a**) 5CSZ, (**b**) 6CSZ, (**c**) 7CSZ, (**d**) 8CSZ, (**e**) 9CSZ, and (**f**) 10CSZ specimens before post-heat treatment (same magnification).

The mechanical properties of Ca-PSZ evaluated by the Vickers hardness and flexural strength of Ca-PSZ are displayed in Figures 4 and 5, respectively. Increasing the CaO content from 5CSZ to 10CSZ increased the Vickers hardness and flexural strength from 676.02 to 1256.25 HV and 437.7 to 842.7 MPa, respectively (see black lines in Figures 4 and 5). As shown by the red lines in Figures 4 and 5, the post-heat treatment enhanced the mechanical properties from 5CSZ to 9CSZ. Vickers hardness increased from 773.58 (5CSZ) to 1201.26 HV (9CSZ), and flexural strength increased from 453.1 (5CSZ) to 827.7 MPa (9CSZ). However, a marginal decrease (approximately 7%) in Vickers hardness (1159.34 HV) and flexural strength (771 MPa) compared to 9CSZ was observed in 10CSZ after the post-heat treatment. Even with the results of 10CSZ, the mechanical properties based on the Vickers hardness and flexural strength tests of the specimens from 5CSZ to 10CSZ were significantly enhanced by increasing the Ca content and applying the post-heat treatment, compared to the previous

study [28]. As expected, the V_m values of all specimens before and after the post-heat treatment decreased, and this was related to the portion of the Ca^{2+} substitution for Zr^{4+}.

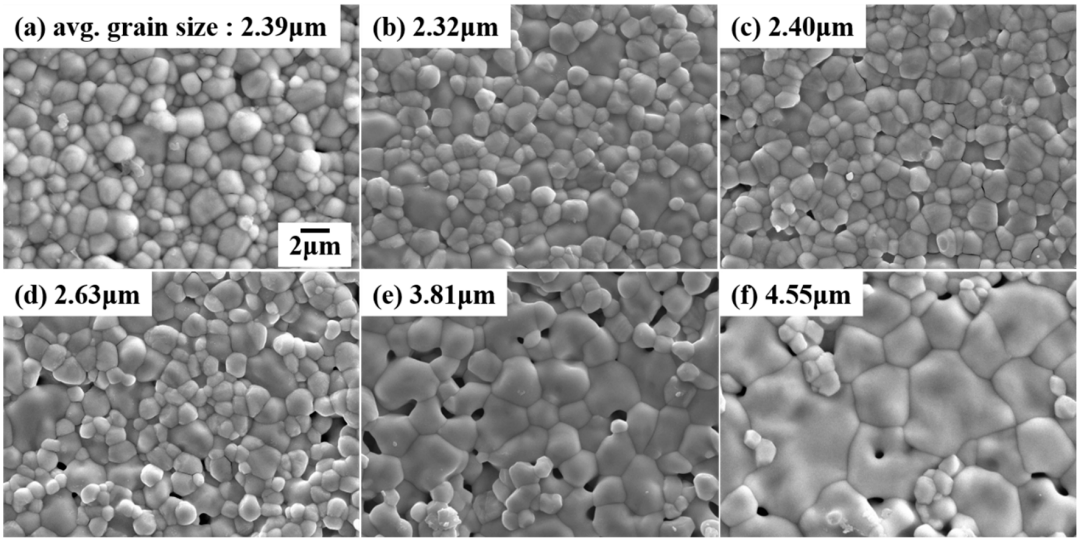


Figure 3. FE-SEM images and average grain sizes of (**a**) 5CSZ, (**b**) 6CSZ, (**c**) 7CSZ, (**d**) 8CSZ, (**e**) 9CSZ, and (**f**) 10CSZ specimens after post-heat treatment (same magnification).

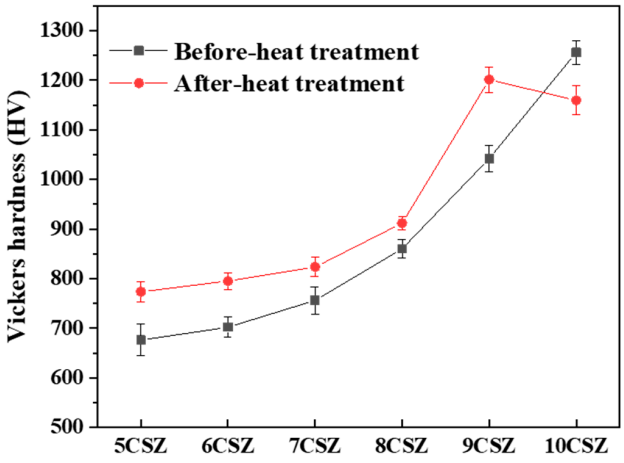


Figure 4. Vickers hardness of Ca-PSZ before (black scattered line) and after (red scattered line) post-heat treatment.

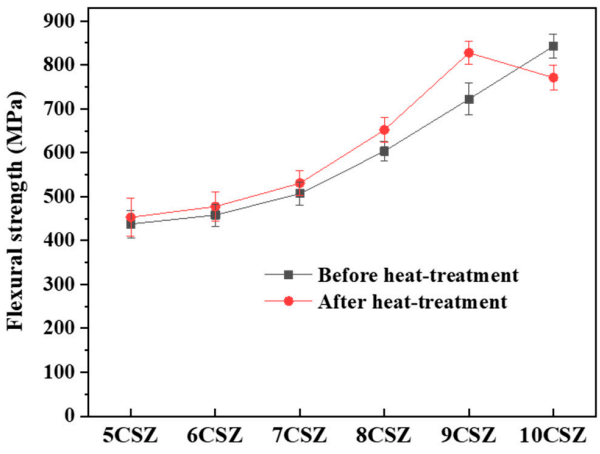


Figure 5. Flexural strength of Ca-PSZ before (black scattered line) and after (red scattered line) post-heat treatment.

The reason the mechanical properties of 10CSZ decreased could be explained by the XRD and SEM analyses. The quantity of Ca^{2+} dissolved in the ZrO_2 lattice increased as the CaO content increased. In addition, this process led to a greater number of formations of oxygen vacancies and facilitated the transition from the monoclinic phase to a stable tetragonal phase [28,32–34]. In addition, it was assumed that the post-heat treatment reduced the number of pores, which are generated during the sintering process, and facilitated the chemical reaction between ZrO_2 and CaO, increasing the bonding strength between the raw particles and improving the mechanical properties of Ca-PSZ [35]. In contrast, a reduction in Vickers hardness and flexural strength in 10CSZ after the post-heat treatment suggests that the high-temperature condition of the post-heat treatment at 1200 °C affected the formation of a balanced-phase $CaZrO_3$, which resulted in some regions of the specimen containing relatively high and low Ca concentrations. This Ca concentration imbalance resulted in an increase in the monoclinic phase, an unstable phase from external forces [36]. Abnormal particle growth may also have contributed to a decrease in mechanical strength. As illustrated in Figure 3, most of particles grew similar in size to 9CSZ, and thus the deviation among the particles was small. However, in 10CSZ, the average particle size increased as compared to other specimens, and there were also many abnormally large particles. It is believed that the grain, which is weaker than the grain boundary in the ceramic specimens, caused the weakening of the mechanical strength due to a large amount of doping of Ca and the overgrowth from the subsequent thermal treatment.

The curve of the thermal expansion coefficient for Ca-PSZ obtained at a temperature range of 30–1000 °C is shown in Figure 6; additionally, the thermal expansion coefficients of each specimen are listed in Table 2. The change in the linear dimension can be estimated by the equation of linear expansion coefficients, Equation (2), as follows:

$$\frac{\Delta L}{L_0} = \alpha_L \Delta T \tag{2}$$

where L_0 is the initial length of the specimen, ΔL is the change in the length, α_L is the coefficient of linear thermal expansion, and ΔT is the temperature change in the specimen. Generally, the thermal expansion coefficient increased as the CaO content increased from 5CSZ (8.229×10^{-6} K^{-1}) to 10CSZ (9.448×10^{-6} K^{-1}); this was enhanced by the post-heat treatment. The post-heat treatment temperature of 1200 °C is the temperature at which the tetragonal phase and the monoclinic phase are transformed, and the heat treatment at this temperature for 100 h is thought to produce sufficient energy and time to change the monoclinic phase to the tetragonal phase. However, the thermal expansion coefficient of the 10CSZ specimen decreased by approximately 4% to 9.086×10^{-6} K^{-1}; this behavior is similar to that shown by the mechanical properties. In general, thermal treatment at high temperatures in zirconia converts the monoclinic phase into a tetragonal phase, resulting in stabilization of mechanical and thermal properties. However, in the case of 10CSZ, the amount of Ca added was large, resulting in the secondary phase such as $CaZrO_3$ and causing a concentration imbalance of Ca, leading to the destabilization of Ca [36,37]. Accordingly, it is believed that the tetragonal phase, which is stable at high temperatures, is reduced, and the thermal expansion coefficient is degraded. Consequently, the thermal property also improved similar to the mechanical properties with the increase in the Ca content from 5CSZ to 10CSZ and the post-heat treatment as compared to the previous study [28]. However, despite all the results being better than the previous results, the 10CSZ specimen after the post-heat treatment showed a different behavior compared to the other specimens (5CSZ to 9CSZ). As briefly explained above, it is believed that if more than 10 mol% of Ca is doped, CaZrO3 would be produced by heat treatment at a phase transformation temperature of 1200 degrees, resulting in the destabilization of Ca-PSZ. In order to obtain better performance of Ca-PSZ at high temperatures, a method to prevent the destabilization of Ca will be required in the future works.

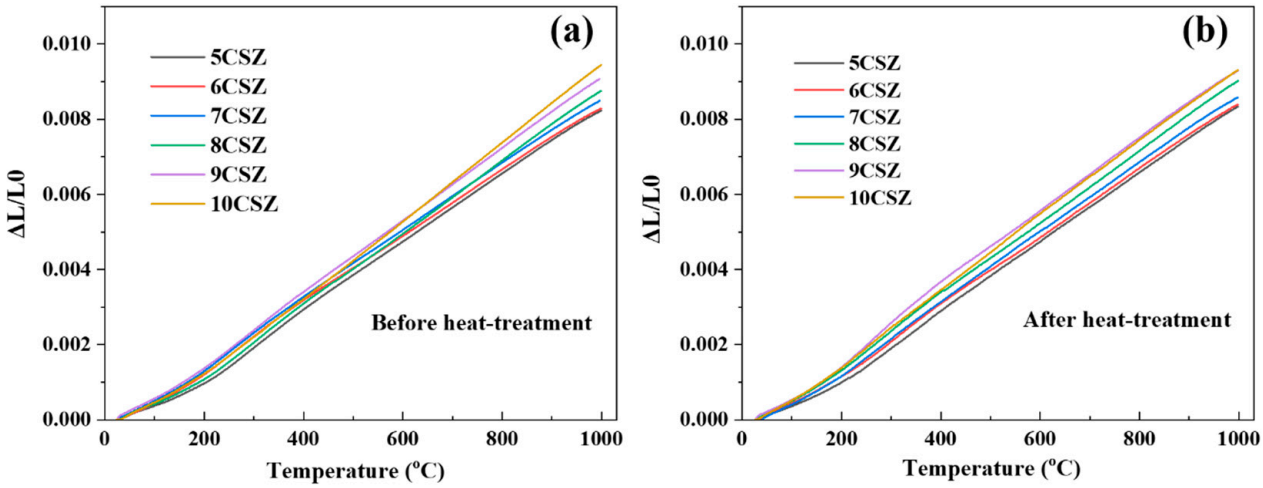


Figure 6. Thermal expansion coefficient curves of Ca-PSZ (**a**) before and (**b**) after post-heat treatment.

Table 2. Thermal expansion coefficient of Ca-PSZ.

Specimen	Thermal Expansion Coefficient (1/K)	
	Before Post-Heat Treatment	After Post-Heat Treatment
5CSZ	8.229×10^{-6}	8.342×10^{-6}
6CSZ	8.288×10^{-6}	8.390×10^{-6}
7CSZ	8.490×10^{-6}	8.588×10^{-6}
8CSZ	8.758×10^{-6}	9.025×10^{-6}
9CSZ	9.074×10^{-6}	9.294×10^{-6}
10CSZ	9.448×10^{-6}	9.086×10^{-6}

4. Conclusions

The effects of the post-heat treatment and varying CaO content on the crystal structure, microstructure, mechanical and thermal properties of Ca-PSZ in the CaO-ZrO_2 system were investigated. The monoclinic phase ratio of the specimens before the post-heat treatment decreased as the CaO content increased from 5CSZ to 10CSZ (62.50%–21.02%), and 9CSZ exhibited the lowest monoclinic phase ratio (19.57%). After the post-heat treatments, 5CSZ to 9CSZ showed further reduction in the monoclinic phase ratio compared to that before the post-treatment; however, this value for 10CSZ increased from 21.02% to 24.84%. There was no significant difference in the average grain size of the specimens that had CaO content from 5CSZ to 8CSZ regardless of the post-heat treatment; however, the average grain size of 9CSZ and 10CSZ significantly increased to 3.64 and 4.55 μm, respectively. Moreover, the grain size increased even further with the post-heat treatment. This seems to be due to the particle size gradient depending on the amount of CaO added and resulting in different growth-driving forces. The mechanical properties were analyzed using the Vickers hardness and flexural strength tests. The thermal property was analyzed using the thermal expansion coefficient. The mechanical and thermal properties improved with the increase in the CaO content before the post-heat treatment. It is believed that the increased oxygen vacancy due to the increase in the CaO addition helped to produce a relatively stable tetragonal phase compared to a monoclinic, low-temperature phase, and it enhanced the mechanical and thermal strength of the specimens.

As a result of the post-heat treatment, the mechanical and thermal properties improved up to 9CSZ as the monoclinic phase ratio decreased. Because the post-heat treatment temperature of 1200 °C is the tetragonal–monoclinic phase transformation temperature, the heat treatment at this temperature for 100 h is thought to produce sufficient energy and time to change the monoclinic phase to the tetragonal phase for the stabilization of CSZ. However, the properties of 10CSZ deteriorated along with the increase in the monoclinic

phase ratio. This was because the CaO-rich $CaZrO_3$ phase was formed as a second phase at the post-heat treatment temperature, which increased the monoclinic phase ratio due to CaO deficiency as shown by the XRD and SEM results.

All results for V_m from 5CSZ to 10CSZ were lower compared to the previous study of 2CSZ to 4CSZ [28], as expected, and this might have affected the enhancement of the mechanical and thermal properties of 5CSZ to 10CSZ, because the decrease in V_m is directly related to these properties. In conclusion, Ca might be a good stabilizer for zirconia, and modification of the Ca content can control the mechanical and thermal properties of Ca-PSZ by changing the volume fraction of the monoclinic and tetragonal phases of zirconia. Moreover, these properties could also be controlled through post-heat treatment since it also changes the volume fraction. For further improvements in mechanical and thermal properties, destabilization of Ca may be required. Co-doping of Ca and other stabilizers is considered as one of the possible methods and will be investigated in future work.

Author Contributions: Conceptualization, H.L. (Hwanseok Lee); data curation, J.K.; formal analysis, H.L. (Hwanseok Lee); funding acquisition, H.L. (Heesoo Lee); investigation, H.Y. and J.K.; methodology, H.L. (Hwanseok Lee); project administration, H.L. (Heesoo Lee); supervision, I.J.; visualization, I.J.; writing—original draft preparation, H.Y. and J.K.; writing—review & editing, I.J. and H.L. (Heesoo Lee). All authors have read and agreed to the published version of the manuscript.

Funding: This work was supported by Korea Institute for Advancement of Technology (KIAT) grant funded by the Korea Government (MOTIE) (P0008335, HDR Program for Industrial Innovation).

Data Availability Statement: The data and analysis in this study are available on request from the corresponding authors.

Conflicts of Interest: The authors declare no conflict of interest.

References

1. Maynard, A. Navigating the fourth industrial revolution. *Nat. Nanotechnol.* **2015**, *10*, 1005–1006. [CrossRef]
2. Daemmrich, A. Invention, innovation systems, and the fourth industrial revolution. *Technol. Innov.* **2017**, *18*, 257–265. [CrossRef]
3. Maksoud, A.; Fahlm, R.; Shala, A.; Elkodous, M.; Olojede, S.; Osman, A.; Farrell, C.; Al-Muhtaseb, A.; Awed, A.; Ashour, A.; et al. Advanced Materials and technologies for super capacitors used in energy conversion and storage: A review. *Environ. Chem. Lett.* **2021**, *19*, 375–439. [CrossRef]
4. Haider, R.; Wen, Y.; Ma, Z.; Wilkinson, D.; Zhang, L.; Yusan, X.; Song, S.; Zhang, J. High temperature proton exchange membrane fuel cells: Progress in advanced materials and key technologies. *Chem. Soc. Rev.* **2021**, *50*, 1138–1187. [CrossRef]
5. Ryan, K.; Down, M.; Banks, C. Future of additive manufacturing: Overview of 4D and 3D printed smart and advanced materials and their applications. *J. Chem. Eng.* **2021**, *403*, 126162. [CrossRef]
6. Lopez-Gandara, C.; Ramos, F.M.; Cirera, A. YSZ-based oxygen sensors and the use of nanomaterials: A review from classical models to current trends. *J. Sens.* **2009**, *2009*, 258489. [CrossRef]
7. Olah, J.; Aburumman, N.; Popp, J.; Khan, M.A.; Haddad, H. Impact of industry 4.0 on environmental sustainability. *Sustainability* **2020**, *12*, 4674. [CrossRef]
8. Hou, X.; Zhao, X.; Zhang, Y.; Zhang, Z.; Liu, Y.; Qin, Y.; Tan, P.; Chen, C.; Yu, S.; Ding, M.; et al. High-Performance Harsh-Environment-Resistant GaOX Solar-Blind Photodetectors via Defect and Doping Engineering. *Adv. Mater.* **2022**, *34*, 2106923. [CrossRef]
9. Manicone, P.F.; Iommetti, P.R.; Raffaelli, L. An overview of zirconia ceramics: Basic properties and clinical applications. *J. Dent.* **2007**, *35*, 819–826. [CrossRef]
10. Loganathan, A.; Gandhi, A. Effect of phase transformations on the fracture toughness of t′ yttria stabilized zirconia. *Mater. Sci. Eng. A* **2012**, *556*, 927–935. [CrossRef]
11. Talibi, M.; Kaur, K.; Parmar, H. Do you know your ceramics? Part 5: Zirconia. *Br. Dent. J.* **2022**, *232*, 311–316. [CrossRef]
12. Juri, A.Z.; Zhang, Y.; Kotousov, A.; Yin, L. Zirconia responses to edge chipping damage induced in conventional and ultrasonic vibration-assisted diamond machining. *J. Mater. Res. Technol.* **2021**, *13*, 573–589. [CrossRef]
13. Yan, M.; Li, Y.; Yin, G.; Tong, S.; Chen, J. Synthesis and characterization of a MgO-$MgAl_2O_4$-ZrO_2 composite with a continuous network microstructure. *Ceram. Int.* **2017**, *43*, 5914–5919. [CrossRef]
14. Gao, L.; Guan, R.; Zhang, S.; Zhi, H.; Jin, C.; Jin, L.; Wei, Y.; Wang, J. As-sintered Manganese-Stabilized Zirconia Ceramics with Excellent Electrical Conductivity. *Crystals* **2022**, *12*, 620. [CrossRef]
15. Li, K.; Jiang, Q.; Chen, J.; Peng, J.; Li, X.; Koppala, S.; Omaran, M.; Chen, G. The controlled preparation and stability mechanism of partially stabilized zirconia by microwave intensification. *Ceram. Int.* **2020**, *46*, 7523–7530. [CrossRef]

16. Li, P.; Cen, I.W. Effect of Dopants on Zirconia Stabilization—An X-ray Absorption. *J. Am. Ceram. Soc.* **1994**, *77*, 1281–1288. [CrossRef]
17. Chen, G.; Ling, Y.; Li, Q.; Zheng, H.; Li, K.; Jiang, Q.; Gao, L.; Omran, M.; Peng, J.; Chen, J. Stability properties and structural characteristics of CaO-partially stabilized zirconia ceramics synthesized from fused ZrO_2 by microwave sintering. *Ceram. Int.* **2020**, *46*, 16842–16848. [CrossRef]
18. Toraya, H.; Yoshimura, M.; Somiya, S. Calibration Curve for Quantitative Analysis of the Monoclinic-Tetragonal ZrO_2 System by X-Ray Diffraction. *J. Am. Ceram. Soc.* **1984**, *67*, 119–121.
19. Kulyk, V.; Duriagina, Z.; Kostryzhev, A.; Vasyliv, B.; Vavrukh, V.; Marenych, O. The Effect of Yttria Content on Microstructure, Strength, and Fracture Behavior of Yttria-Stabilized Zirconia. *Materials* **2022**, *15*, 5212. [CrossRef]
20. Chen, P.; Li, X.; Tian, F.; Liu, Z.; Hu, D.; Xie, T.; Liu, Q.; Li, J. Fabrication, microstructure, and properties of 8 mol% yttria-stabilized zirconia (8YSZ) transparent ceramics. *J. Adv. Ceram.* **2022**, *11*, 1153–1162. [CrossRef]
21. Yusuf, D.; Maryani, E.; Mardhian, D.; Noviyanti, A. Evaluation of Structural Stability, Mechanical Properties, and Corrosion Resistance of Magnesia Partially Stabilized Zirconia (Mg-PSZ). *Molecules* **2022**, *28*, 6054. [CrossRef]
22. Juyoung, K.; Buyoung, K.; Heesoo, L. Technology development trends related to zirconia materials. *J. Korean Inst. Electr. Electron. Mater. Eng.* **2020**, *33*, 18–30.
23. Zhang, M.; Gao, L.; Kang, J.; Pu, J.; Peng, J.; Omran, M.; Chen, G. Stability optimisation of CaO-doped partially stabilized zirconia by microwave sintering. *Ceram. Int.* **2019**, *45*, 23278–23282. [CrossRef]
24. Hwanseok, L.; Kanghee, J.; Heesoo, L. Phase stability of yttria-stabilized zirconia under thermo-chemical stressfor solid oxide membrane electrolysis. *J. Surf. Sci. Eng.* **2021**, *6*, 38.
25. Li, K.; Chen, J.; Peng, J.; Koppala, S.; Omran, M.; Chen, G. One-step preparation of CaO-doped partially stabilized zirconia from fused zirconia. *Ceram. Int.* **2020**, *46*, 6484–6490. [CrossRef]
26. Changsu, H. Degradation of ZrO_2-C Material for Submerged Entry Nozzle in Thin Slab Casting. *J. Korean Ceram. Soc.* **1998**, *35*, 251–258.
27. Tsubakino, H.; Nozato, R.; Hamamoto, M. Effect of Alumina Addition on the Tetragonal-to-Monoclinic Phase Transformation in Zirconia–3 mol% Yttria. *J. Am. Ceram. Soc.* **1991**, *74*, 440–443. [CrossRef]
28. Yoo, H.J.; Lee, H.S.; Jo, K.H.; Kim, J.Y.; Jo, I.K.; Lee, H.S. Phase Formation and Stabilization Behavior of Ca-PSZ by Post-Heat Treatment. *Metals* **2022**, *12*, 1479. [CrossRef]
29. Heuer, A.H.; Claussen, N.; Kriven, W.M.; Ruhle, M. Stability of Tetragonal ZrO_2 Particles in Ceramic Matrices. *J. Am. Ceram. Soc.* **1982**, *65*, 642. [CrossRef]
30. Evis, Z.; Ergun, C.; Doremus, R.H. Hydroxylapatite-zirconia composites: Thermal stability of phases and sinterability as related to the CaO-ZrO_2 phase diagram. *J. Mater. Sci.* **2005**, *40*, 1127–1134. [CrossRef]
31. Leib, E.W.; Pasquarelli, R.M.; Rosario, J.J.; Dyachenko, P.N.; Doring, S.d.; Puchert, A.; Petrov, A.U.; Eich, M.; Schneider, G.A.; Janssen, R.; et al. Yttria-stabilized zirconia microspheres: Novel building blocks for high-temperature photonics. *J. Mater. Chem. C* **2016**, *4*, 62–74. [CrossRef]
32. Eugenio, F.; Lucia, G. Oxygen vacancy formation and their role in the CO_2 activation on Ca doped ZrO_2 surface: An *ab-initio* DFT study. *Appl. Surf. Sci.* **2021**, *553*, 149589.
33. Lu, X.; Liang, K.; Gu, S.; Zheng, Y.; Fang, H. Effect of oxygen vacancies on transformation of zirconia at low temperatures. *J. Mater. Sci.* **1997**, *32*, 6653–6656. [CrossRef]
34. Kurumada, M.; Hara, H.; Iguchi, E. Oxygen vacancies contributing to intragranular electrical conduction of yttria-stabilized zirconia (YSZ) ceramics. *Acta Mater.* **2005**, *53*, 4839–4846. [CrossRef]
35. Jihoon, P.; Ilhwan, B.; Sangjin, L. Phase Transition and Thermal Expansion Behavior of Zirconia Setter Fabricated from Fused CaO Stabilized Zirconia. *J. Korean Ceram. Soc.* **2019**, *56*, 184–190.
36. Jung, J.H.; Yon, S.J.; Seok, J.W. Cubic zirconia single crystal growth using shell by skull melting method. *J. Korean Cryst. Growth Cryst. Technol.* **2013**, *23*, 124–128. [CrossRef]
37. Guo, X. Property Degradation of Tetragonal Zirconia Induced by Low-Temperature Defect Reaction with Water Molecules. *Chem. Mater.* **2004**, *16*, 3988–3994. [CrossRef]

Disclaimer/Publisher's Note: The statements, opinions and data contained in all publications are solely those of the individual author(s) and contributor(s) and not of MDPI and/or the editor(s). MDPI and/or the editor(s) disclaim responsibility for any injury to people or property resulting from any ideas, methods, instructions or products referred to in the content.